Int. J. Nano Dimens. 2026; 17(3) : 325-332

International Journal of Nano Dimension (IJND)

https://doi.org/10.57647/ijnd.2026.1703.05

Original Research

Silver Oxide and Silver Iodide Nanomaterials Through the Green Synthesis from *Acacia Senegal* Plant and Biocompatibility Their Use as Anti-Liver Cancer Agents

Saad I. Esmail, Ali Bahari*

Department of Physics, Faculty of Science, University of Mazandaran, Babolsar, Iran

***Corresponding author:** a.bahari@umz.ac.ir

Article History

Received:
8 October 2025

Revised:
2 December 2025

Accepted:
3 December 2025

Published online:
2 January 2026

Published in Issue:
10 July 2026

Abstract:

Silver iodide (AgI) can be obtained from *Acacia Senegal* and has the potential to inhibit cancer growth. The present investigation using relevant techniques, can be used for the liver cancer (HePG2) in the cell line treatment with silver oxide (AgO) nano-crystallites. This was achieved by exposing Liver cancer cell (HePG2) and healthy cells (WRL68) to 25,50,100,200, and 400 µg/mL concentrations of AgO. The novelty of the present study is comparison of the two types of cells: The (HePG2) and (WRL68) to the (AgI) from *A. Senegal* plant, which to our knowledge has not been reported. We also used the IC_{50} assay, which is a measurement used to describe the effectiveness of a substance in inhibiting or suppressing a specific enzyme or cell activity. The IC_{50} value represents the concentration of the substance required to inhibit the target biological activity by 50%. The graph in Figure shows an IC_{50} value of 70 in liver cancer cells, which is a positive result. However, the IC_{50} value in healthy cells was somewhat low at 193. These are good results because the lower the IC_{50} value in cancer cells, the better the outcome, and the opposite should be true for healthy cells.

Keywords: Anti-liver cancer activities; Green synthesis; Nano crystallites; Silver oxide (AgO); Silver iodide (AgI)

Cite this article: Esmail SI, Bahari A. Silver Oxide and Silver Iodide Nanomaterials Through the Green Synthesis from *Acacia Senegal* Plant and Biocompatibility Their Use as Anti-Liver Cancer Agents. Int. J. Nano Dimens. 2026;17(3): 325-332. https://doi.org/10.57647/ijnd.2026.1703.05

1. Introduction

The scientific community has showing increasing interest in Nano biotechnology for its potential applications in biomedicine, including diagnostics, biomolecule sensing, disease inhibition and treatments [1, 2, 3, 4, 5]. Metallic nanoparticles (NPs), including gold, zinc, silver (Ag), iron, and copper, have found numerous applications in the medical field over the past decades [5]. In particular, the unique physicochemical and visual characteristics of silver nanoparticles (AgNPs) make them a promising therapeutic agent [6]. These procedures are risky, costly, and cumbersome to manage in bulk. The green synthesis procedure is a novel approach that has the potential to address these challenges [7]. The biological synthesis of silver nanoparticles (AgNPs) has numerous advantages over traditional techniques [7]. These attributes include simplicity, environmental friendliness, biocompatibility, efficacy, non-toxicity, cost-effectiveness, and biodegradability in plants. Given their accessibility and high productivity, they are preferred over microbes as a source [6]. Polysaccharides, flavonoids, terpenoids, and other polyphenolic secondary metabolites present in plant extracts facilitate the stabilization and reduction of AgNPs produced [8]. This capping prevents NPs from aggregating and causing harm. To produce pure Ag, biological components reduce silver salts such as (AgI), silver oxide (AgO), and silver (Ag^+) Plants such as *A. Senegal* have medicinal uses [5]. People have long recognized its antibacterial, anti-inflammatory, and wound-healing properties [9]. Its gel and leaf extracts contain a variety

of metabolites, including polysaccharides, proteins, enzymes, terpenoids, flavonoids, vitamins, and phenols [9]. This is attributable to its diverse chemical contents. The anticancer properties of AgNPs have received extensive research attention [10]. The functional groups on NPs enhance their anticancer effect and reduce their toxicity, according to researchers who investigated their mode of action against cancer cells [10]. Furthermore, AgNPs possess intrinsic antioxidant characteristics due to their ability to scavenge free radicals. By neutralizing reactive oxygen species and free radicals produced by damaged or dead cells, these antioxidants provide a healthy glow to the body's cells [11]. The ability of nanoparticles (NPs) to scavenge free radicals is enhanced by plant components, including tannins, herbs, and flavonoids [11]. Chronic illness and mortality may be caused by bacterial infections [11]. Ag, an antibacterial agent, has several applications [12]. AgNPs synthesized using plant extracts exhibit enhanced antibacterial activities [12]. The dimensions of the NPs can be precisely controlled during synthesis to enhance their aggregation at the designated location [13]. A notable advantage of using AgNPs as an anticancer agent is their increased cytotoxicity toward cancer cell types, particularly for small particles. AgNPs possess antibacterial properties because of their interaction with thiol group molecules present in the respiratory base of bacterial cells, rendering them harmful to pathogens [14]. Organic dyes are widely utilized in various industries, including textiles, plastics, and pharmaceuticals, contributing significantly to pollution [15]. Methylene blue, Congo red, methyl orange, and methyl red are some of the hazardous synthetic dyes that AgNPs can degrade because of their promising catalytic activity [16, 17, 18, 19, 20]. We examined the anticancer and anti-oxidative effects of AgNPs on HePG2 liver cancer cell lines. We also analyzed the effect of AgNPs on healthy cells, WRL68, and compared the results with their effect on cancerous cells [17].

2. Materials and method

2.1 Preparation of thin films

Although the applications differed, we employed the same technique in this study as described in our previous work [17]. In this step, *A. Senegal* is usually harvested during the dry season, which begins in October and ends in May. It is then stored for two weeks before being used. To achieve high quality, focus on harvesting the plant during the dry season. The plant should also be stored in dry, cool places. We used 4 g of fresh *A. Senegal* seeds, which were pulverized into a fine powder by using an electric mixer to create a water-based plant extract. Also 1 g of the resulting soluble powder was placed in a heat-resistant flask. Subsequently, 100 mL of distilled water was added to above mixture. A magnetic stirrer was used to combine the powder and supplementary water at 50 °C for 30 min. Thereafter, filter paper was used to purify the plant extract. For the green synthesis process, a solution of (AgI), with a molecular weight of 234.77 g/mol, was created by dissolving 1.17385 g of AgI to achieve a concentration of 0.05 mol. The substance was dissolved in 100 mL of ethanol. To expedite the dissolution process, we added 5 mL of hydrochloric acid to the solution. Finally, a magnetic stirrer was employed to gradually introduce 30 mL of plant extract at 40 °C into the droplets. We terminated the reaction when the color shifted from yellow to blackish-yellow (Fig. 1).

2.2 Synthesis procedure of AgI samples

To successfully precipitate the (AgI) and (AgO) Nano crystallite solution via drop casting, we heated the glass substrates to 70 – 110 °C. A digital thermocouple was affixed to an electric heater, and three drops of the solution were deposited onto glass slides. The slides were then left to sit for 30 min. The sample structures and characteristics are studied with using some relevant techniques such as including X-ray diffraction (XRD), ultraviolet–visible (Uv–Vis) spectroscopy, Fourier transform infrared (FTIR) spectroscopy, field emission scanning electron microscopy (FESEM), and high resolution transmission electron microscopy (HRTEM). We confirmed the material's identification and the presence of NPs by comparing it with the global standard JCPDS. Figure 2 shows the drop-casting technique for material deposition.

3. Results and discussions

3.1 Nanostructural characteristics of the samples with XRD

XRD was used to investigate the structural properties of thin films and the crystallite's phases of the present samples. The application of an NP solution by drop casting onto a glass substrate heated to 70 °C produced a thin layer with evenly distributed NPs, which were used in the fabrication of AgO nanostructures. Figure 3 displays the XRD patterns of (a) AgO, (b) AgI nano

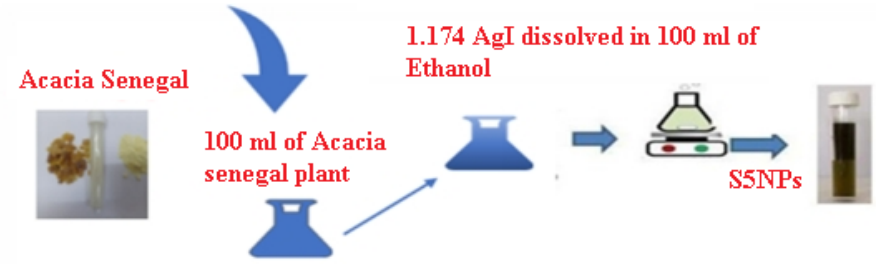

Figure 1. The schematic illustration of the method for silver oxide production.

https://doi.org/10.57647/ijnd.2026.1703.05

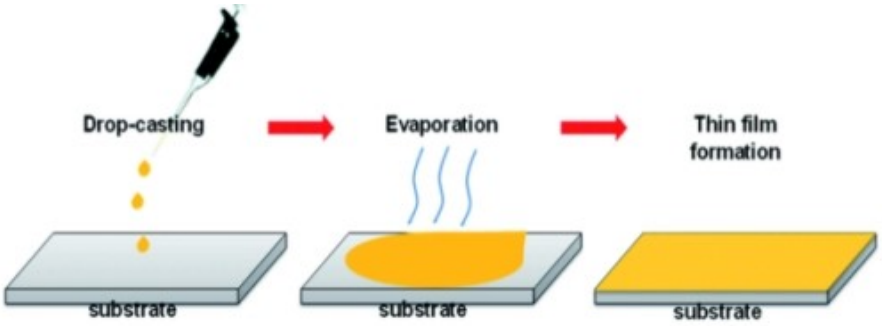

Figure 2. The schematic illustration of the drop-casting method.

crystallites, (c) Williamson-Hall diagram of AgO and (d) Williamson-Hall diagram of AgI, which indicated that the polycrystalline structure of AgI and AgO, with hexagonal and cubic phases, respectively. The peaks (2θ, *hkl*) corresponding to the dominated peaks identified in card number (98-000-1899). Crystallite size with Scherrer method and lattice strain (ε) with Williamson-Hall method is obtained by Eqs. (1) and (2), respectively:

$$D = \frac{K\lambda}{\beta \cos\theta} = \frac{0.9(0.154\ \text{nm})}{(\text{FWHM})\cos\theta} \quad (1)$$

$$\beta_{\text{Sample}} = \beta_{\text{Crystallite Size}} + \beta_{\text{Lattice Strain}} = \frac{K\lambda}{D\cos\theta} + \varepsilon\frac{4\sin\theta}{\cos\theta}$$

$$\beta_{(hkl)}\cos\theta = \frac{K\lambda}{D} + 4\varepsilon\sin\theta \quad (2)$$

In Fig. 3 (c,d), the lattice strain (ε) is estimated by drawing the slope line of the graph for AgO (Fig. 3 (c)) and AgI (Fig. 3 (d)) sample, in that ε for AgO and AgI is 0.089 and 0.025. The lattice strain of the sample is due to different kinds of defects like point defects, grain boundaries, stacking faults, and plasmon. ε value indicates that the mechanical stability of the AgI sample structure with lower ε, is better than that AgO sample. We therefore try to study more AgI in AgO matrix sample for anti-liver cancer agents (as discussed latter in the present work).

Some significant data of the sample are outlined in Tables 1, 2, which give a comparison of the AgO and AgI sample characteristics.

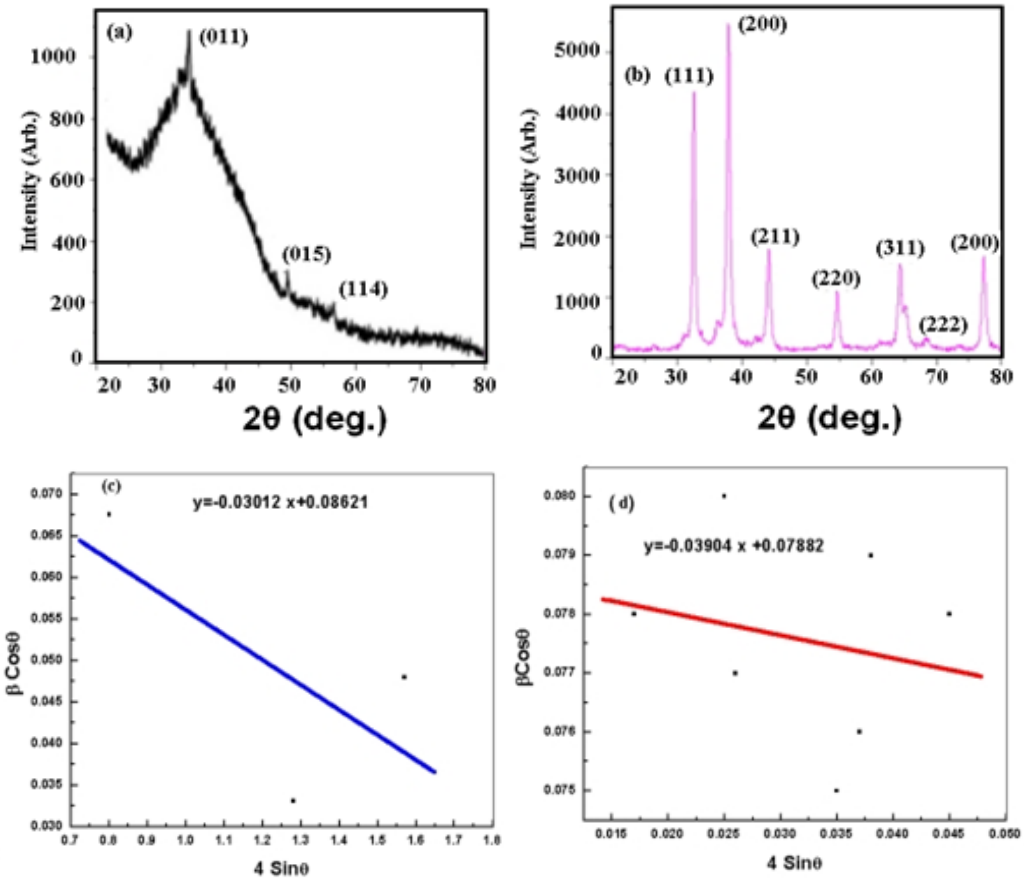

Figure 3. XRD pattern of (a) AgI, (b) AgO nano crystallites, (c) Williamson-Hall diagram of AgO and (d) Williamson-Hall diagram of AgI.

https://doi.org/10.57647/ijnd.2026.1703.05

Table 1. Sample characteristics of AgI, estimated with Eq. (1).

2θ (°)	θ (°)	$\beta_{(hkl)}$ (Rad)	$\beta_{(hkl)} \cos\theta$	D (nm)
23.088	11.544	0.064	0.0676	20.5
37.459	18.730	0.035	0.0331	41.9
46.258	23.130	0.052	0.0480	28.9

Table 2. Sample characteristics of AgO, estimated with Eq. (1).

2θ (°)	θ (°)	$\beta_{(hkl)}$ (Rad)	$\beta_{(hkl)} \cos\theta$	D (nm)
33.000	16.500	0.081	0.078	17.8
37.501	18.800	0.086	0.080	17.3
44.200	22.100	0.083	0.077	18.0
55.000	27.500	0.084	0.075	19.8
64.201	32.100	0.090	0.076	18.2
66.802	33.401	0.095	0.079	19.8
77.400	38.700	0.099	0.0785	17.7

3.2 Topography analysis of the sample surface by Atomic force microscopy (AFM)

To study the matrix sample (AgO) surface topography, two (2D)-, three (3D)- dimension AFM images shown in figure 4. The 3D AFM images, shown in Fig. 4 (a), produced by the environmentally friendly approach of synthesizing AgO NPs exhibited a flat orientation with peaks pointing upwards. The sample topography of the sample surface, shown in Fig. 4 (b), indicated a maximum of 29.4047 nm and an average of 10.6842 nm sample surface roughness .A root mean square (RMS) of 2.04015 nm was calculated for the average surface roughness with Nano Surf software tool. As shown in Fig. 4, the grains were evenly distributed over the 1000 nm × 1000 nm scanning region. The 3D scans revealed that the grains had a semi-spherical morphology with excellent dispersibility. It is clear from the AgO sample surface topography image, it is completely homogeneous and well-oriented vertically.

3.3 Morphology analysis of the sample surface by Field emission scanning electron microscopy (FESEM)

FESEM analysis was conducted to examine the morphology of NPs. From figure 5; FE-SEM images display biosynthesized (AgO) thin films, extracted from *A. Senegal* plant, deposited on a glass substrate via drop-casting method: The image scale (a) 500 scale, (b) 200 nm scale, and in Fig. 5 (c) the size of some crystallites, and Fig. 5 (d) size distribution of AgO nano crystallites, the size distribution of AgO nano crystallites is approximately 29.8 nm. It exhibits that defects like point defects, grain boundaries, and stacking faults, can cause the reduction of the carrier mobility, which is unwanted for present anti-cancer activity due to trap density. But for finding the role of the issue, sample surface plasmon, we will try to use UV-Vis technique.

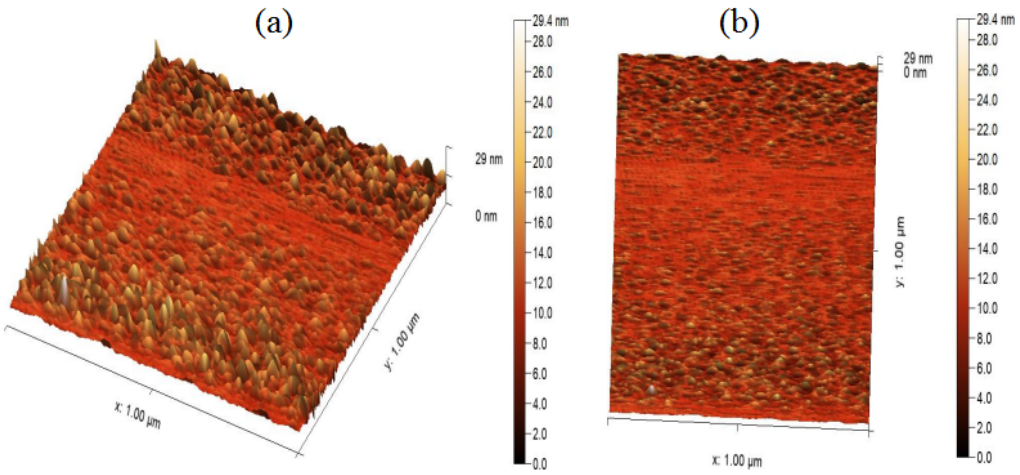

Figure 4. (a) 3D AFM (b) 2D (sample surface) AFM images silver oxide nanoparticles.

https://doi.org/10.57647/ijnd.2026.1703.05

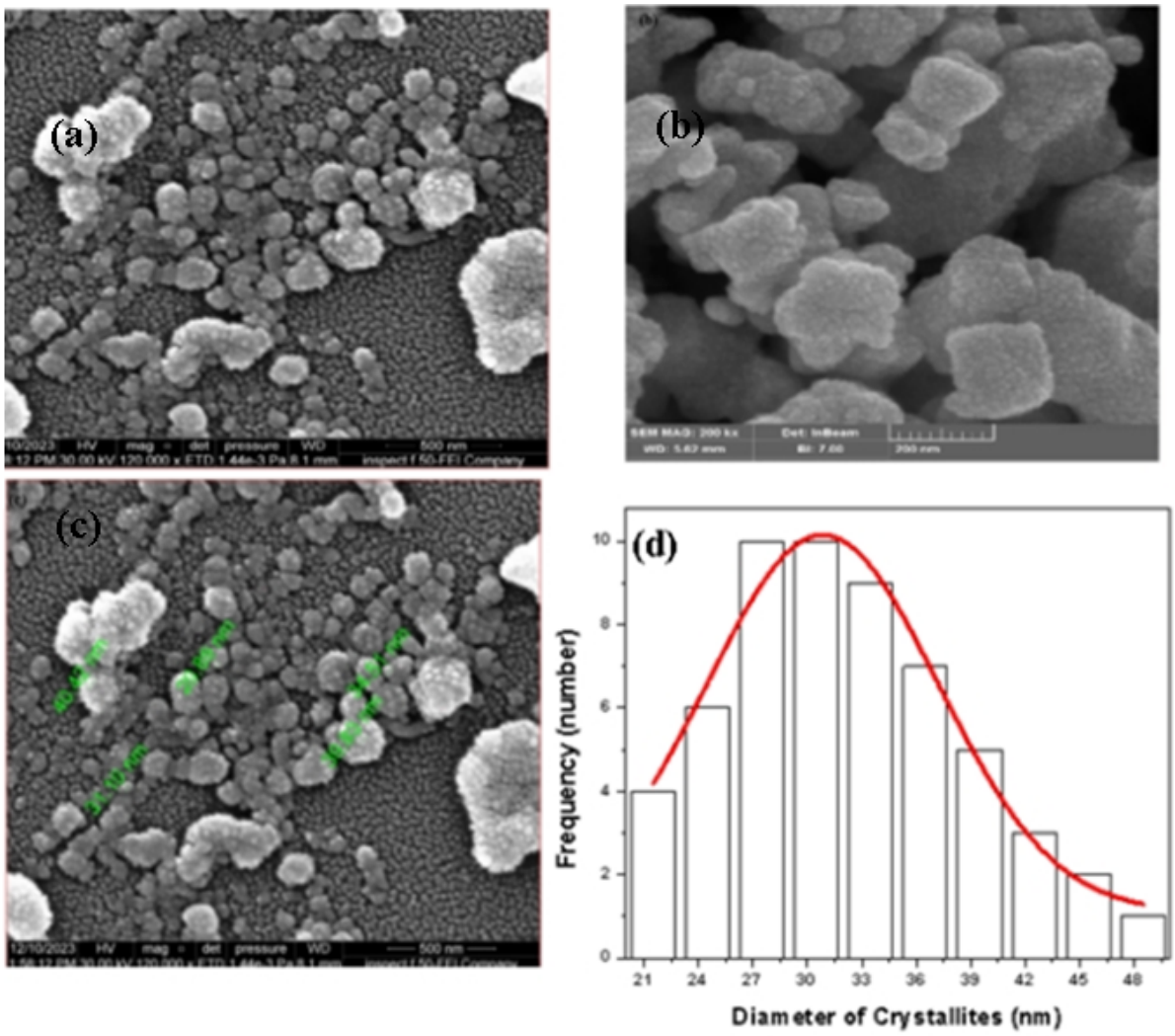

Figure 5. FE-SEM images of the silver oxide nano-crystallites synthesized with Acacia senegal plant extract (a) 500 scale, (b) 200 nm scale, (c) the size of the some crystallites, and (d) Size distribution of AgO nano crystallites.

3.4 The chemical bonding of the AgO with Fourier transform infrared (FTIR) technique

Figure 6 illustrates the FTIR spectrum of the synthesized (AgO) NPs extracted from *A. Senegal* plant. The OH vibrational mode is indicated by a peak at 3450 cm^{-1} in the spectrum. The overtone band vibrations of C_2 corresponded to the peaks observed at 2100 – 2500 cm^{-1}. The C-O band vibrations corresponded to the prominent peak at 1700 cm^{-1}. Also, in Fig. 6, the peak at 690 cm^{-1} was ascribed to the vibrations of the C-H band. The FTIR spectrum confirmed the presence of methylene, carbon, and hydroxide dioxide, all of which are organic compounds that demonstrate the effectiveness of green synthesis.

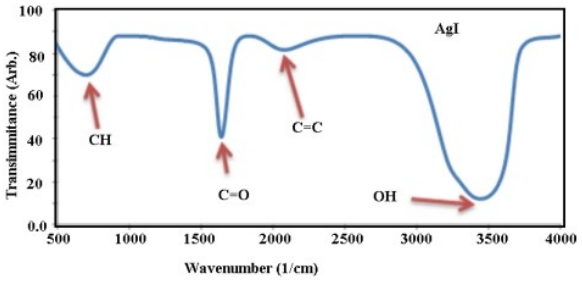

Figure 6. Fourier transform infrared spectrometer silver oxide spectrum.

3.5 Analysis inside structure of the AgO and AgI samples with High-resolution transmission electron (HRTEM)

We observed clearly visible semi-spherical NPs in the HRTEM images of the (AgO) and (AgI) nano composites. Figure 7 (a) shows that the average size of the AgO nanocrystals is around 50 nm, whilst the average size of the AgI nanocrystals is about 20 nm, with different geometry in the crystallite shape.

3.6 UV–Vis spectroscopic analysis

The UV–Vis spectra of AgO NPs synthesized from eco-friendly materials are shown in figure 8. AgO (Fig. 8 (a)) and AgI (Fig. 8 (b)) exhibited dominated peak at 425, and 205 nm in the spectra, respectively. In Fig. 8 (b), other peak at 325 nm -wavelength, could be attributed to the rod-form of the sample surface plasmon peak

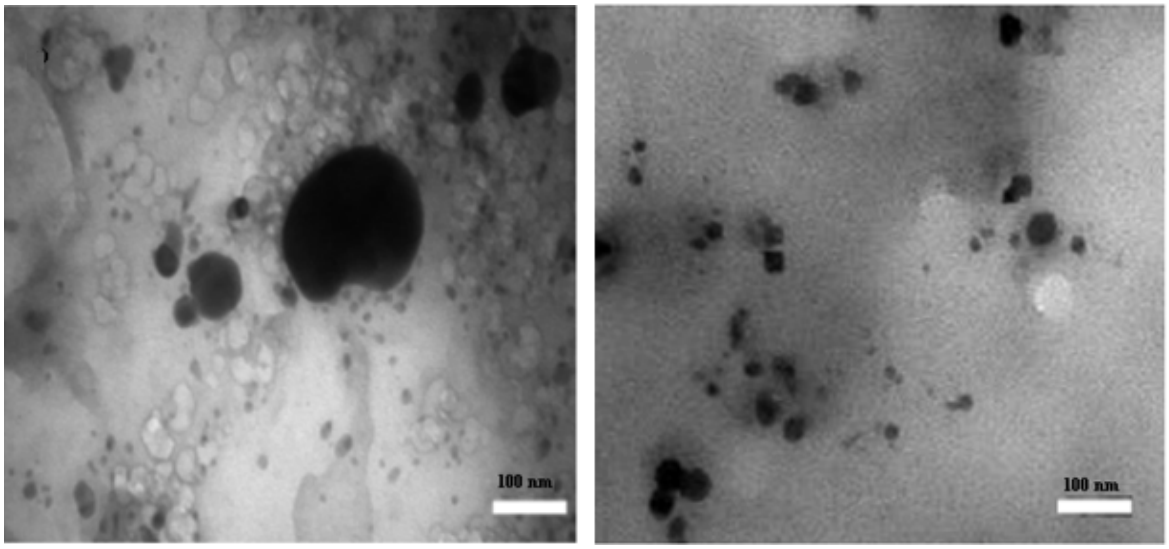

Figure 7. HRTEM images of (a): AgO and (b): AgI.

[18]. The absorption peak of the AgO and AgI curves decreased sharply after about 500 nm- wavelength. One UV–Vis absorption band was associated with the surface plasmon resonance of AgI can be seen with regarding to the Phytochemicals such as flavonoids and polyphenols possess O-H moieties, which causes to the sample to be enable for absorbing UV radiation.

3.7 Anticancer activities of AgI matrix with AgO

In this work, we used (AgO) material derived from (AgI). At this stage, we added varying amounts of AgO to the (WRL68) and (HePG2), and the amount of AgO was determined by MTT assay. We found that the chemical influenced cells, especially cancer cells, as shown in Table 3, where the viability rate dropped to 65% at a dose

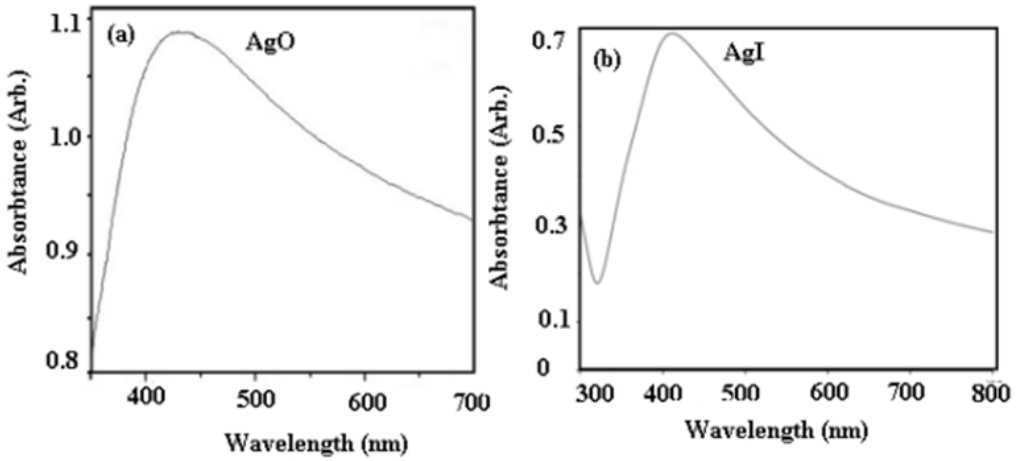

Figure 8. UV–Vis spectrum of (a) AgO and (b) AgI.

Table 3. The cytotoxic effect of silver oxide on WRL68 and HePG2 cell line.

Concentration (µgm/L) S5	Mean viability (%) ± SD WRL68	Mean viability (%) ± SD HePG2
400	63.46467 ± 3.662502	25.077 ± 1.771563
200	76.42767 ± 2.338475	31.48133 ± 1.1575
100	90.66333 ± 1.226403	40.818 ± 2.239414
50	94.213 ± 0.834547	55.01533 ± 1.881241
25	95.83333 ± 0.417689	65.12333 ± 1.428106

https://doi.org/10.57647/ijnd.2026.1703.05

of 25 µg/mL. The most significant effect was observed in AgO as the concentration of silver in the compounds increased. The lowest viability was observed at 400 µg/mL, with 25% viability at elevated dosages. This is due to silver's high toxicity and enhanced efficacy. At 400 µg/mL [16, 17], the effect on healthy cells was minimal, resulting in a viability of 37%. The graph in Fig. 9 indicates a favorable outcome with an IC_{50} value of 70 in liver cancer cells. In healthy cells, the IC_{50} value was 193, which was slightly low. In a recent study conducted by Saeed M Feyadh, et al. (2022) [21], silver iodide (AgI) and silver (Ag) nanoparticles were successfully synthesized using a chemical co-precipitation technique. These nanomaterials were subsequently utilized in MTT cell line assays to evaluate their efficacy against thyroid cancer cells (FTC133). The results revealed that the cytotoxic effect IC_{50} of (AgNPs) was 52.74 µg/mL, whereas that of (AgI) nanoparticles was 95.22 µg/mL. These values were determined using the MTT test on FTC133 cells, indicating a notable difference in their cytotoxic potency. Notably, our research findings are in good agreement with the results of this study, demonstrating similar trends and reinforcing the potential of these nanomaterials in cancer therapy [21].

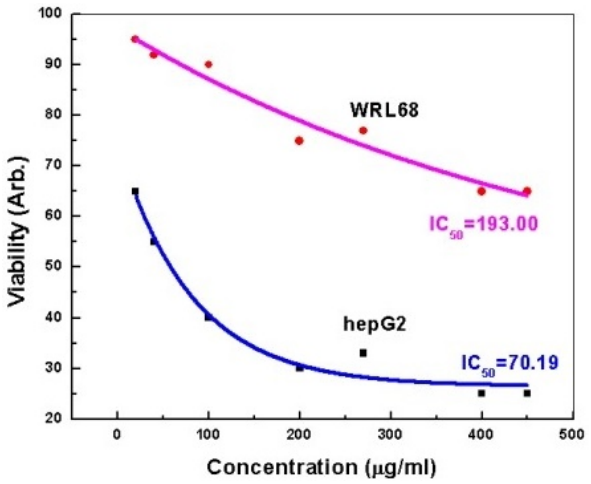

Figure 9. Cell viability rate of syntheses silver oxide Nps concentration of (2550, 100, 200, 400) µg/ with HePG2 cell, and WRL68 cell mL.

4. Conclusions

Nanocrystals of (AgO) or (AgI) can be synthesized via environmentally friendly methods, as demonstrated in this work. The XRD, FTIR, and UV–Vis spectra collectively confirmed the synthesis of AgO nanocrystallites. The presence of hydroxide, carbon dioxide, and methylene, which are organic components that demonstrate the effectiveness of the green synthesis process, was also verified by the FTIR spectrum. At 250 nm, the UV–Vis spectra showed that AgO exhibited a plasmon resonance peak. The AgO nanocrystallites depicted in the FESEM images exhibited sizes of around 40.42, 39.83, 34.51, 31.10, and 20.89 nm, characterized by a semi-spherical surface morphology. The TEM images revealed that the nanocrystals had a size of around 50 nm. The AFM scans showed RMS of the average surface roughness was 2.04015 nm. Researchers have used AgO nanocrystals as an anticancer agent, yielding mixed results. At various doses, they demonstrated significant activity against (HepG2) cells, a human liver cancer cell line.

Authors contributions
All authors contributed equally to the conception, design, execution, and writing of this work. All authors read and approved the final manuscript.

Availability of data and materials
The authors declare that the data supporting the findings of this study are available within the paper.

Conflict of interests
The authors assert that they do not have any identifiable conflicting financial interests or personal relationships that might be perceived to influence the work presented in this paper.

References

1. Vaishali K, Nirmala M, Pavithra N, and Balakrishnan K. "Sol gel synthesis of undoped and Nitrogen doped Titanium Dioxide nanoparticles as nano fertilizer for plant growth. " Int. J. Nano Dimens. 2024; 15(4):1524301–8. DOI: 10.57647/j.ijnd.2024.1504.30
2. Azari B, Pourahmad A, Sadeghi B, and Mokhtary M. "Green synthesis of SiO_2 from Equisetnm arvense plant for synthesis of SiO_2/ZIF-8 MOF nanocomposite as photocatalyst. " Journal of Coordination Chemistry 2023; 76(2):219–231. DOI: 10.1080/00958972.2023.2166408
3. Oves M, Rauf MA, Aslam M, Qari HA, Sonbol H, Ahmad I, Zaman GS, and Saeed M. "Green synthesis of silver nanoparticles by Conocarpus-lancifolius plant extract and their antimicrobial and anticancer activities. " Saudi Journal of Biological Sciences 2023; 29(2):460–471. DOI: 10.1016/j.sjbs.2021.09.007
4. Al-Hakkani MF. "Biogenic copper nanoparticles and their applications: A review. " SN Applied Sciences 2020; 2(3):505–15. DOI: 10.1007/s42452-020-2199-4
5. Sutradhar P, Saha M, and D.Maiti. "Microwave synthesis of copper oxide nanoparticles using tea leaf and coffee powder extracts and its antibacterial activity." Journal of Nanostructure in Chemistry 2024; 4:86–99. DOI: 10.1007/s40097-014-0086-0
6. Konduri VV, Kalagatur NK, Gunti L, Mangamuri UK, Kalagadda VR, Poda S, and Krishna SBN. "Green synthesis of silver nanoparticles from Hibiscus tiliaceus L. leaves and their applications in dye degradation, antioxidant, antimicrobial, and anticancer activities." South African Journal of Botany 2024; 168:476–487. DOI: 10.1016/j.sajb.2024.03.035

7. Wang Y and Wei S. "Green fabrication of bioactive silver nanoparticles using Menthapulegium extract under alkaline conditions: An enhanced anticancer activity. " ACS Omega. 2022; 7(2):1494–1504. DOI: 10.1021/acsomega.1c05473
8. Govindappa M, Tejashree S, Thanuja V, Hemashekhar B, Srinivas C, Nasif O, Pugazhendhi A, and Raghavendra V. "Pomegranate fruit fleshy pericarp mediated silver nanoparticles possessing antimicrobial, antibiofilm formation, antioxidant, biocompatibility and anticancer activity. " Journal of Drug Delivery Science and Technology 2021; 61:102289–97. DOI: 10.1016/j.jddst.2020.102289
9. Alattar AM. "The influence of pulsed laser on the structural and optical properties of green tea extract leaf produced with silver nanoparticles as antimicrobial. " Journal of Molecular Liquids 2024; 398:124287. DOI: 10.1016/j.molliq.2024.124287
10. Mbenga Y, Adeyemi JO, Mthiyane DMN, Singh M, and Onwudiwe DC. "Green synthesis, antioxidant and anticancer activities of TiO_2 nanoparticles using aqueous extract of Tulbhagia violacea." Results Chem 2023; 6:101007–17. DOI: 10.1016/j.rechem.2023.101007
11. Al Baloushi KSY, Senthilkumar A, Kandhan K, Subramanian R, J. K, Ramachandran T, Shehab S, Kurup S, Alyafei M, Dhaheri ASA, and Jaleel A. "Green synthesis and characterization of silver nanoparticles using Moringaperegrina and their toxicity on MCF-7 and Caco-2 human cancer cells. " International Journal of Nanomedicine 2024; 19:3891–3905. DOI: 10.2147/IJN.S451694
12. Basavarajappa DS, Kumar RS, Almansour AI, Chakraborty B, Bhat MP, Nagaraja SK, Hiremath H, Perumal K, and Nayaka S. "Biofunctionalized silver nanoparticles synthesized from Passifloravitifolia leaf extract and evaluation of its antimicrobial, antioxidant and anticancer activities." Biochemical Engineering Journal 2022; 182:108517–27. DOI: 10.1016/j.bej.2022.108517
13. Younis AB, Haddad Y, Kosaristanova L, and Smerkova K. "Titanium dioxide nanoparticles: Recent progress in antimicrobial applications." WIREs Nanomedicine Nanobiotechnology 2023; 15:e1860–77. DOI: 10.1002/wnan.1860
14. Rudrappa M, Kumar RS, Nagaraja SK, Hiremath H, Gunagambhire PV, Almansour AI, Perumal K, and Nayaka S. "Myco-nanofabrication of silver nanoparticles by Penicilliumbrasilianum NP5 and their antimicrobial, photoprotective and anticancer effect on MDA-MB-231 breast cancer cell line. " Antibiotics 2023; 12(3):567–276. DOI: 10.3390/antibiotics12030567
15. Hublikar LV, Ganachari SV, Patil VB, Nandi S, and Honnad A. "Anticancer potential of biologically synthesized silver nanoparticles using Lantana camara leaf extract. " Progress in Biomaterials 2023; 12(2):155–169. DOI: 10.1007/s40204-023-00219-9
16. Nguyen LAT, Mai BV, Nguyen, Thi Nguyen DV, Pham NQ, Pham VV, and Le TLM. "Green synthesis of silver nanoparticles using Callisiafragrans leaf extract and its anticancer activity against MCF-7, HepG2, KB, LU-1, and MKN-7 cell lines. " Green Processing and Synthesis 2024; 12(1):20230024–34. DOI: 10.1515/gps-2023-0024
17. Bahari A, Esmail SI, and Alattar AM. "Investigate optical and structural properties with molecular behavior of AgI and silver oxide nanoparticles prepared by green synthesis from the Acacia Senegal plant and achieving biocompatibility. " Journal of Optics 2024; 54(3):1261–1268. DOI: 10.1007/s12596-024-01810-4
18. Shajari D, Bahari A, Gill P, and Mohseni M. "Synthesis and tuning of gold nanorods with surface plasmon resonance. " Optical Materials 2017; 64:376–83. DOI: 10.1016/j.optmat.2017.01.004
19. Muthuvel A, Said NM, Jothibas M, Gurushankar K, and Mohana V. "Microwave-assisted green synthesis of nanoscaled titanium oxide: photocatalyst, antibacterial and antioxidant properties." Journal of Material Science Material Electronic 2021; 32:23522–23539. DOI: 10.1007/s10854-021-06840-3
20. Bahari A, Ahmady-Asbchin S, Naeij M, Farhadikoutenaei A, and Al-Jilef A. "Green synthesis and study of structural properties of Copper nanocrystallites from hawthorn plant extract and study of its antibacterial activities." Int. J. Nano Dimens. 2023; 14(2):138–44. DOI: 10.22034/ijnd.2023.1977078.2199
21. Feyadh SM and Mohammed AH. "Syntheses, characterization, and suppression efficiency of silver & silver iodide nanoparticle for proliferation, migration, and invasion in follicular thyroid carcinoma cells. " Mater Res Express 2022; 9:055402. DOI: 10.1088/2053-1591/ac6d4b